Bifurcations of a semiclassical atom in a periodic field

Thomas Pohl,[1] Ulrike Feudel,[2] and Werner Ebeling[1]
[1]*Institute of Physics, Humboldt-University Berlin, Invalidenstrasse 110, D-10115 Berlin, Germany*
[2]*ICBM and Department of Physics, Carl von Ossietzky University Oldenburg, PF2503, 26111 Oldenburg, Germany*
(Received 1 August 2001; revised manuscript received 27 November 2001; published 10 April 2002)

The dynamics of an electron moving in the Coulomb field of a nucleus and a strong periodic field is studied in a semiclassical model. Hamiltonian equations of motion are derived using Gaussian wave functions, a variational principle, and an adiabatic approximation for the width of the wave packets. Predictions for the ionization probability are found to agree rather well with exact calculations in the barrier supression regime. By introducing dissipation and fluctuation the model atom is considered as an open system. For the dissipative system we investigate the bifurcations in dependence on strength and frequency of the external field. A quite complex bifurcation scenario is obtained. The sensitivity with respect to noise is also studied.

DOI: 10.1103/PhysRevE.65.046228 PACS number(s): 05.45.Pq, 03.65.Sq, 02.30.Oz

I. INTRODUCTION

Many experimental and theoretical studies of periodically driven atoms have been made to understand a variety of features, e.g., higher harmonic generation or stabilization phenomena [1,2]. The classical electron dynamics plays an important role in the investigation of highly excited atomic electrons in a periodical field [3]. The underlying potential especially for one-dimensional calculations has to have several properties—the absence of the singularity at the origin and the asymptotic Coulomb-like behavior. A widely used form that satisfies these conditions is the so-called ''soft-core potential''

$$V(\mathbf{r}) = \frac{1}{\sqrt{r^2+\varepsilon^{-2}}}. \tag{1}$$

Here ε is the ground-state energy of the atom. Many other choices satisfying the above conditions are possible.

From a time-dependent variational principle we derive an adiabatic Hamiltonian describing the motion of a semiclassical electron. This Hamiltonian differs slightly from Eq. (1). Note that Eq. (1) is an *ad hoc* introduced potential, whereas the semiclassical adiabatic approximation (SAA) presented in this paper follows from physical principles. In the following we investigate the semiclassical electron dynamics for different kinds of atomic potentials. We will analyze in detail the bifurcations in dependence on the electric field strength and the frequency of the external laser field. It will be shown that slight differences in the shape of the potential lead to drastic changes in the dynamics of the system.

II. HAMILTONIAN DYNAMICS

A. Semiclassical approximation

The Hamiltonian operator describing a one-electron atom in a periodical field is given by

$$\hat{H} = \frac{\hat{\mathbf{p}}}{2} - \frac{Z}{r} + V(\hat{\mathbf{r}},\hat{\mathbf{p}},t). \tag{2}$$

For all further calculations we use atomic units ($e = m_e = \hbar = 1$). The laser field is treated in the dipole approximation, where only linearly polarized light is considered

$$\hat{V}(\mathbf{r},t) = \mathbf{E}_0 \cdot \mathbf{r} \sin \omega t. \tag{3}$$

Here the vector $\mathbf{E}_0$ defines the direction and the amplitude of the external field. One possible semiclassical description of this problem is based on an approximation for the particle wave function containing time-dependent parameters $q(t)$, which represent the coordinates in a generalized phase space. This technique has been widely applied in quantum molecular dynamics to study problems in plasma physics [4–9] and nuclear physics [10,11]. The dynamics of the parameters is described by the time-dependent variational principle [12]

$$\delta \int_{t_1}^{t_2} \langle \psi | i \frac{d}{dt} - \hat{H} | \psi \rangle dt = 0. \tag{4}$$

The equations of motion can be written in the general form [12]

$$\dot{q}_\mu = \sum_\nu A^{-1}_{\mu\nu} \frac{\partial H}{\partial q_\nu}, \tag{5}$$

where the Hamiltonian function H is defined as the expectation value of the Hamiltonian $\hat{H}$

$$H = \langle \psi | \hat{H} | \psi \rangle. \tag{6}$$

As a trial wave function we choose a Gaussian wave packet

$$\psi(\mathbf{q};\mathbf{r},\mathbf{p},\beta,p_\beta) = \left(\frac{3}{2\pi\beta}\right)^{3/4} \exp\left[-\left(\frac{3}{4\beta} + i p_\beta\right)(\mathbf{q}-\mathbf{r})^2 - i\mathbf{p}\cdot(\mathbf{q}-\mathbf{r})\right]. \tag{7}$$

Here β and p_β parametrize the complex width of the distribution, while $\mathbf{r}$ and $\mathbf{p}$ are the average position and average momentum, respectively. With this choice of the wave function the matrix $A^{-1}_{\mu\nu}$ is of canonical form

$$A_{\mu\nu}^{-1}=\begin{pmatrix}0 & -1\\ 1 & 0\end{pmatrix}, \tag{8}$$

which leads to a Hamiltonian-like dynamics for the parameters with the following semiclassical Hamiltonian:

$$H=\frac{p^2}{2}-\frac{Z}{\mathbf{r}}\,\mathrm{erf}\left(\mathbf{r}\sqrt{\frac{3}{2\beta}}\right)+2p_\beta^2\beta+\frac{9}{8\beta}+\mathbf{E}_0\cdot\mathbf{r}\sin\omega t. \tag{9}$$

If the electric field is chosen to be directed along the r_3 axes $[\mathbf{r}=(r_1,r_2,r_3)]$ and cylindric coordinates are introduced ($x=r_3$, $y=\sqrt{r_1^2+r_2^2}$, $\tan\phi=r_2/r_1$), we obtain from the Hamiltonian [Eq. (9)] the following equations of motion:

$$\begin{aligned}
\dot{x}&=p_x,\\
\dot{p}_x&=-Z\frac{x}{r^3}\left[\mathrm{erf}\left(r\sqrt{\frac{3}{2\beta}}\right)-\sqrt{\frac{6}{\pi\beta}}\,r\exp\left(-\frac{3r^2}{2\beta}\right)\right]\\
&\quad+E_0\sin(\omega t),\\
\dot{y}&=p_y,\\
\dot{p}_y&=-Z\frac{y}{r^3}\left[\mathrm{erf}\left(r\sqrt{\frac{3}{2\beta}}\right)-\sqrt{\frac{6}{\pi\beta}}\,r\exp\left(-\frac{3r^2}{2\beta}\right)\right],\\
\dot{\beta}&=4p_\beta\beta,\\
\dot{p}_\beta&=\frac{9}{8\beta^2}-2p_\beta^2-Z\sqrt{\frac{2}{2\pi\beta^3}}\exp\left(-\frac{3r^2}{2\beta}\right).
\end{aligned} \tag{10}$$

Using this form of dynamical equations the width of the wave packet provides an additional degree of freedom. This fact leads to a divergent partition sum and to wrong predictions for the thermal capacity fulfilling neither the classical nor the quantum limit. Thus, modifications of Eq. (10) are necessary to solve these problems. The simplest possibility is to fix the width at the value that gives the minimum ground-state energy. Introducing a new parameter $r_0^2=2\beta/3$, this condition is fulfilled for

$$r_0=\frac{3}{4Z}\sqrt{\pi} \tag{11}$$

with a groundstate energy of $\varepsilon_0=-0.424Z^2$, which is about 15% higher than the exact value provided by quantum mechanics. From the fixed width arises the problem, that the ionization energy obtained from Eq. (9) does not agree with quantum-mechanical predictions. The third summand in Eq. (9), the so-called curvature energy, leads to an ionization energy of $\varepsilon_B=0.848Z^2$.

In order to avoid these difficulties we introduce a SAA, which is based on the assumption of a slowly varying width of the wave packet. From the condition $p_\beta=0$ we find for given r and p the following expression for r_0:

$$r_0=\frac{3}{4Z}\sqrt{\pi}\exp\left(\frac{r^2}{r_0^2}\right). \tag{12}$$

This adiabatic approximation solves the problem of the wrong ionization energy as well as the problems of the additional degree of freedom. To get an explicit expression for the width of the wave packet we expand Eq. (12) in r_0 and obtain

$$r_0=\tfrac{3}{8}\sqrt{\pi}+\tfrac{1}{8}\sqrt{9\pi+64r^2}. \tag{13}$$

For testing the result we perform the limit $Z\to 0$, which corresponds to a free electron in a linearly polarized laser field. By substituting the solution of Eq. (10) in Eq. (7) we obtain the Volkov wave function in the long wavelength approximation

$$\psi=\exp\left(i\mathbf{p}\cdot\mathbf{r}-i\frac{p^2}{2}t-i\frac{E_0^2}{4\omega^2}t+i\frac{E_0p_x}{\omega^2}\sin\omega t-i\frac{E_0^2}{8\omega^3}\sin 2\omega t\right), \tag{14}$$

which is the exact quantum-mechanical solution for the problem. As mentioned above the SAA predicts an ionization energy that is smaller than the exact energy provided by exact quantum theory. With respect to this property the SAA seems to be worse than the soft-core potential to describe atom light interactions. However, the atomic potential should also give good predictions for the polarizability of the atom, defined by

$$\alpha=\frac{p}{E}, \tag{15}$$

where p is the dipole moment resulting from the static electric field E. Quantum-mechanical perturbation theory predicts for the hydrogen ground state a value of $\alpha=4.5$ a.u. Using a harmonic expansion of the semiclassical potentials the polarizability can be estimated by $\alpha=e^2/\omega_0^2$. The soft-core potential fitted to the exact ground-state energy yields $\alpha=8$ a.u., which is about two times higher than the exact value. Our SAA potential based on a Gaussian wave packet leads to $\alpha=3.1$ a.u., which is only 30% of the exact value.

B. Free oscillations

The equations of motion [Eq. (10)] can be rescaled to the atomic hydrogen case by the substitutions

$$\begin{aligned}
&\tilde{x}=Zx,\quad \tilde{y}=Zy,\quad \tilde{\beta}=Z^2\beta,\\
&\tilde{p}_x=Zp_x/Z,\quad \tilde{p}_y=Zp_y/Z,\quad \tilde{p}_\beta=p_\beta/Z^2,\\
&\tilde{E}_0=E_0/Z^3,\quad \tilde{\omega}=\omega/Z^2,\quad \tilde{t}=Z^2t.
\end{aligned} \tag{16}$$

For that reason we will consider the case of a hydrogen atom $Z=1$ for all further calculations. Figure 1(a) shows the shape of the SAA potential compared to the ''soft-core'' potential.

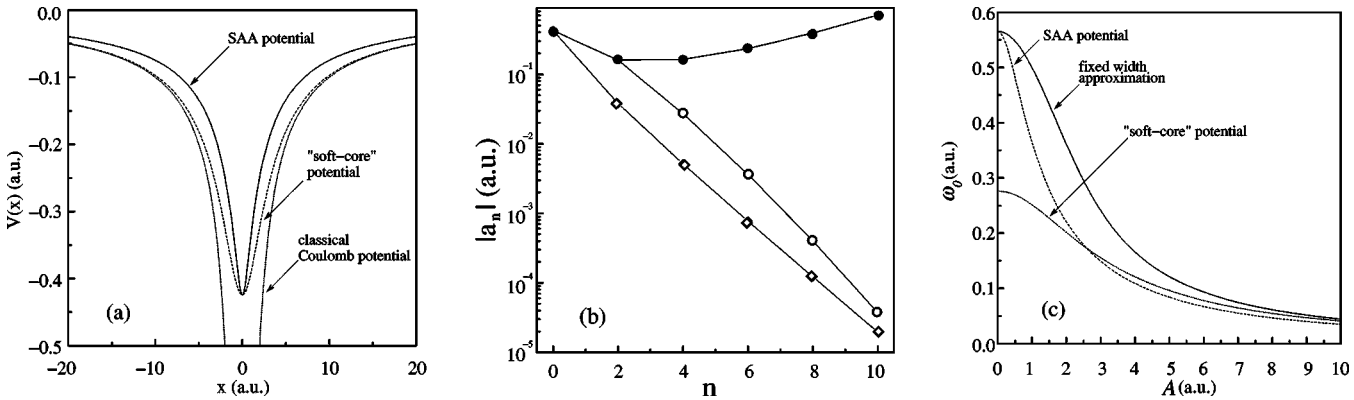

FIG. 1. Comparison of certain properties of different atomic potentials. The spatial shape (a), the leading coefficents in a Taylor expansion (b) and the frequency of free linear oscillations as a function of the corresponding amplitude are shown for different types of potentials. In (b) the results for the three potentials derived from Eq. (1) (diamonds), Eqs. (9),(11) (open circles), and Eqs. (9),(13) (full circles) are shown.

The principle shape of both potentials looks very similar. But a more detailed analysis of the short distance behavior, given by the leading coefficients α_k in a Taylor expansion [Fig. 1(b)], as well as the asymptotic behavior shows significant differences, which may lead to very different dynamical behavior at high and low energies. Furthermore, the relatively good agreement of the coefficients α_k for the potentials derived from Eqs. (11) and (13) gives rise to the expectation of similar dynamics at small distances. The asymptotic behavior of the ''soft-core'' potential is given by

$$V(r) = -\frac{1}{r} + \frac{8r_0^4}{9}\frac{1}{r^3} - \frac{32r_0^8}{27}\frac{1}{r^5} + \cdots, \tag{17}$$

whereas the potentials derived from the variational principle converge to $-Z/r$ exponentially. As we will show processes, such as ionization or stabilization phenomena, are dominated by the asymptotic behavior, whereas the higher harmonic spectrum is caused by the shape of the potential at short distances [3]. Using the Lindstedt-Poincaré method the main frequency of the one-dimensional free oscillations can be expanded as [13]

$$\omega = \sqrt{\tilde{\alpha}_1}\left(1 + \frac{9\tilde{\alpha}_1\tilde{\alpha}_3 - 10\tilde{\alpha}_2^2}{24\tilde{\alpha}_1^2}A^2 + \cdots\right), \tag{18}$$

where A is the amplitude of the single harmonic term in the solution and $\tilde{\alpha}_k$ are coefficients in a Taylor series of the atomic force. A comparison of the eigenfrequencies for the three potentials is given in Fig. 1(c).

C. The action of the external field

The action of strong external fields gives rise to essential changes of the atomic dynamics. The approximation proposed here reduces the problem to the classical dynamics in an oscillating two-dimensional potential well. As shown above, in the limit of very large fields or for $Z \to 0$ the model is exact, since the Volkov wave function is reproduced. For smaller fields however, the electron feels the details of the atomic model potential. Due to the different degree of nonlinearitiy of the ''soft-core'' and the other two potentials a periodic perturbation applied to these atomic forces will lead to different results. To prove this we use a stroboscopic Poincaré plot of the perturbed trajectories. The initial conditions are choosen in a way as to obtain oscillations along the polarization direction of the electric field ($y = p_y = 0$). For the potentials described by Eqs. (9) and (11) and by Eqs. (9) and (13) we found two different resonant orbits, where one orbit corresponds to the inner black dots in Fig. 2(a). The other orbit lies outside of Fig. 2(a) similar to that one in Fig. 2(b). The transition in form of chaotic layers between the two

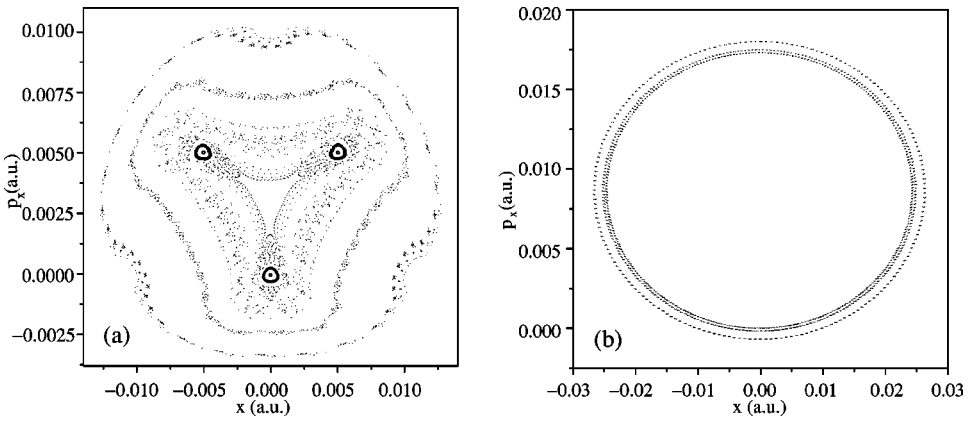

FIG. 2. Stroboscopic Poincaré plot for different initial conditions for the potentials calculated from Eqs. (9) and (13) (a) and Eq. (1) (b) for $E_0 = 0.01$ a.u. and $\omega = 0.1$ a.u.

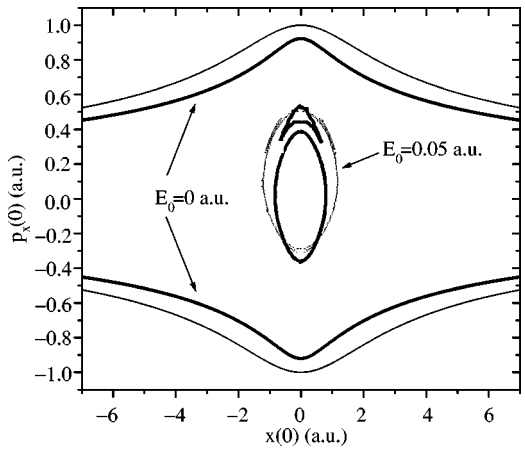

FIG. 3. Separatrix corresponding to closed orbits and open trajectories derived for the ''soft-core'' potential (thin lines) and for the SAA potential (thick lines).

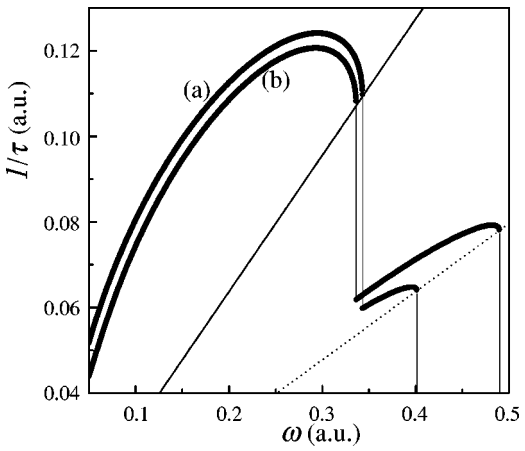

FIG. 4. Ionization rate as a function of external frequency for the ''soft-core'' (a) and the SAA potential (b) for a field strength of $E_0=0.2$ a.u. The inverse times $2/T$ (solid line) and $1/T$ (dotted line) are also shown.

orbits is also shown. For the ''soft-core'' potential neither ultraharmonic nor subharmonic resonance has been observed in this parameter regime. The corresponding single harmonic orbits are shown in Fig. 2(b). Due to $1/\mathbf{r}$ behavior of the potentials, the phase space is divided into two regions corresponding to closed orbits and open trajectories diverging to infinity. If an external field is applied, a transition between a closed orbit and the open trajectories may occur. During some cycles of the external field an amount of energy is transferred to the electron until it escapes over the barrier formed by the atomic field and the laser field. As mentioned above the potential derived from Eq. (9) is not very useful to describe ionization processes. That is why we consider only the ''soft-core'' and the ''adiabatic appoximation'' potential. Such a separatrix, which divides the space of initial conditions into two parts of bound and free motions, for an instantaneously switched on field at $t=0$ is shown in Fig. 3 for two different external field strengths, where $y=p_y=0$. Here the electron is considered as ionized if its energy without the contribution of the external field changes to positive values. We see again that different atomic potentials can lead to much different results. The asymmetry of the separatrix for finite fields arises from the initial phase ϕ of the external field, which is set to $\phi=0$ for the calculations in Fig. 3. If one considers the phase of the field as an additional degree of freedom the separatrix becomes symmetric in this higher-dimensional space.

For an investigation of the ionization process in more detail we measured the time needed for a transition from a bounded to an unbounded state. This time is estimated by the time τ at which the energy of the electron changes to positive values. The inverse of this characteristic time gives an estimation of the ionization rate in this semiclassical picture. The resulting dependence on the external frequency for both potentials is shown in Fig. 4. The simulations were started from the atomic ground state that corresponds to $\mathbf{p}(0)=\mathbf{r}(0)=0$. One can see that for both potentials a stabilization takes place at higher frequencies of the external field due to a dynamical trapping of the electron. For a critical frequency ω_c, the ionization rate decreases rapidly. Here the electron is bound for half of a cycle of the external field longer than for $\omega<\omega_c$. At this frequency the electron energy becomes positive exactly after one half cycle $T=2\pi/\omega$ of the external field. For frequencies larger than ω_c the electron is slowed down by the field at $t>T/2$ due to the phase difference between the electron motion and the external electric field. This leads to the rapid decrease of the ionization rate beyond ω_c. For a further increasing frequency the ionization rate increases until the electron motion is again in phase with the external field. The inverse times $2/T$ and $1/T$ are also shown in Fig. 4 to underline the above statements. This dynamical stabilization is purely a classical effect. In a recent work a method similar to the Feynman path-integral formalism has been developed to describe the electron energy spectrum in the final state [14]. These calculations are based on classical electron trajectories weighted with a complex number whose phase is equal to the classical action along the trajectory. The observed energy spectrum of the ejected electrons is very well described by this theory. This shows that the classical electron motion is essential for certain effects of atom-light interaction. Thus, we expect that the classical stabilization effect plays a role in quantum-mechanical ionization processes. As can be seen from Fig. 4 both atomic potentials lead, in principle, to the same ionization behavior. But, again there are quantitative differences between both atomic models. In some frequency interval the ionization rate calculated from the SAA model is less than the rate obtained with the ''soft-core'' potential although the binding energy of the ''soft-core'' potential is larger than for the SAA potential. This means that the study of ionization of atoms by strong laser fields as done in [2] with the ''soft-core'' potential as well as the investigation of the higher harmonic spectrum [3] depend on the choice of the underlying atomic model.

D. Comparison with quantum calculations

In order to check the validity of the proposed model we will compare the predicted ionization behavior of the semiclassical model atom with numerical solutions of the time-

dependent Schrödinger equation. Additionally, the results will be compared with quantum results for the Coulomb-free case [15] to demonstrate the importance of the Coulomb interaction. The definition of the ionization rate used above has been successfully applied to the problem of electron impact ionization in plasmas [8]. Since quantum effects become more important for the case of photon electron interaction, no quantitative agreement with quantum-mechanical calculations can be expected. However, the dynamical trapping described above should also occur in more realistic calculations, and might be the reason for discrepancies between the numerically calculated ionization rates and the quasistatic theory in the barrier supression regime [16]. The importance of this classical effect might be proven by numerical investigations of the time-dependent Schrödinger equation.

The main reason for possible discrepancies with exact investigations is the fact that the used wave packets can only have one maximum. Thus, tunneling cannot be described within this model. But for sufficiently large fields, the electron is able to escape over the barrier formed by the Coulomb potential and the laser field. This so-called barrier suppression ionization (BSI) is much faster than tunneling, which is dominant for weaker fields. In this regime, classical and semiclassical pictures have been found to work well [15,17]. The probability to find the electron in its atomic ground state at the time t is given by

$$P(t)=|\langle\psi(\mathbf{x},0)|\psi(\mathbf{x},t)\rangle|^2, \tag{19}$$

where $\psi(\mathbf{x},\mathbf{0})$ is the ground-state wave function. Using Eq. (7) for the time-dependent wave function, we get

$$P(t)=\left(\frac{36\beta_0\beta}{D}\right)^{3/2}\exp\left\{\frac{-3}{2D}[(9B+p_\beta C)r^2 + 4\beta_0\beta B p^2 - C\mathbf{r}\cdot\mathbf{p}]\right\}. \tag{20}$$

Here $\beta_0=27\pi/32Z^2$ follows from Eq. (11) and $B=\beta_0+\beta$, $C=16p_\beta\beta_0\beta^2$ and $D=9B^2+p_\beta\beta_0 C$. From this equation we calculate the ground-state population as a function of time by evaluating the parameters according to Eq. (10) with $\mathbf{r}(\mathbf{0})=\mathbf{p}(\mathbf{0})=p_\beta(\mathbf{0})=\mathbf{0}$ and $\beta(0)=\beta_0$ to obtain the best possible ground-state properties. In [18] the three-dimensional time-dependent Schrödinger equation has been solved numerically, for the problem of an one-electron atom in a linearly polarized laser field. In this work the authors found a simple semiempirical formula for $P(t)$ by a fit to their numerical solution. To compare our result with this formula, we apply the pulse shape used in [18]

$$E(t)=E_0\sin\omega t\exp\left(-\frac{(t-t_0)^2}{\sigma^2}\right), \tag{21}$$

where $t_0=N\pi/\omega$ and $\sigma^2=t_0^2/\ln 20$. In Fig. 5 we compare our results with the formula of Bauer and Mulser [18] for different laser pulses. For a ground-state population larger than 50%, the degree of agreement is similar to that with the exact solution of the Schrödinger equation (see [18]). For

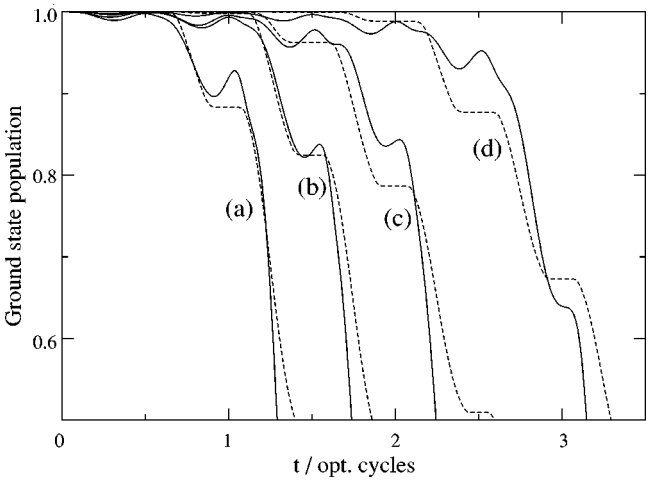

FIG. 5. Comparison between the time dependence of the ground-state population obtained from Eq. (20) and the quantum result found in [18], for $E_0=0.5$, $N=6$, $\omega=0.2$ (a), $E_0=0.3$, $N=6$, $\omega=0.2$ (b), $E_0=0.5$, $N=12$, $\omega=0.2$ (c) and $E_0=0.3$, $N=12$, $\omega=0.2$ (d). The time is shown in units of the period length of the external field.

$P(t)<0.5$ the ground-state population given by Eq. (20) decreases to fast with increasing time. This is mainly due to the fact that the ground-state properties of the atom at large distances from the core are not very well described by the Gaussian approximation.

Let us now study the properties of the light emitted by the oscillating electron. In [15] it has been shown that in the BSI regime even the first laser cycle gives the main contribution to the dipole acceleration, which is known to directly determine the coherent part of the emitted light spectral energy

$$E_\omega\propto|\ddot{\mathbf{d}}_\omega|^2, \tag{22}$$

where ω is the frequency of the emitted light, E_ω is the energy per frequency, and

$$\ddot{\mathbf{d}}_\omega=\int_0^\infty\ddot{\mathbf{d}}(t)e^{i\omega t}dt \tag{23}$$

is the Fourier transform of the dipole acceleration. Since we have shown that in the BSI regime the wave packet model does describe the ionization process for this time interval, we expect that the emission of light can also be described within the proposed model. According to the wave packet model the expectation value of the operator of the dipole acceleration $\partial_{tt}\hat{\mathbf{d}}(t)=Z\mathbf{x}/x^3-\mathbf{E}(t)$ is given by

$$\ddot{\mathbf{d}}(t)=-\mathbf{E}(t)-\boldsymbol{\nabla}V_{eff}(r), \tag{24}$$

where the effective potential is given by

$$V_{eff}(\mathbf{r})=-\frac{Z}{\boldsymbol{r}}\,\mathrm{erf}\left(\frac{r}{\rho}\right), \tag{25}$$

and the parameters $\mathbf{r}$ and $\rho=\sqrt{2\beta/3}$ are determined by Eq. (10) with $\mathbf{r}(\mathbf{0})=\mathbf{0}$ and $\rho(0)$ is given by Eq. (11). In [15] the dipole acceleration for the BSI regime has been calculated by an expansion in terms of the interatomic Coulomb potential

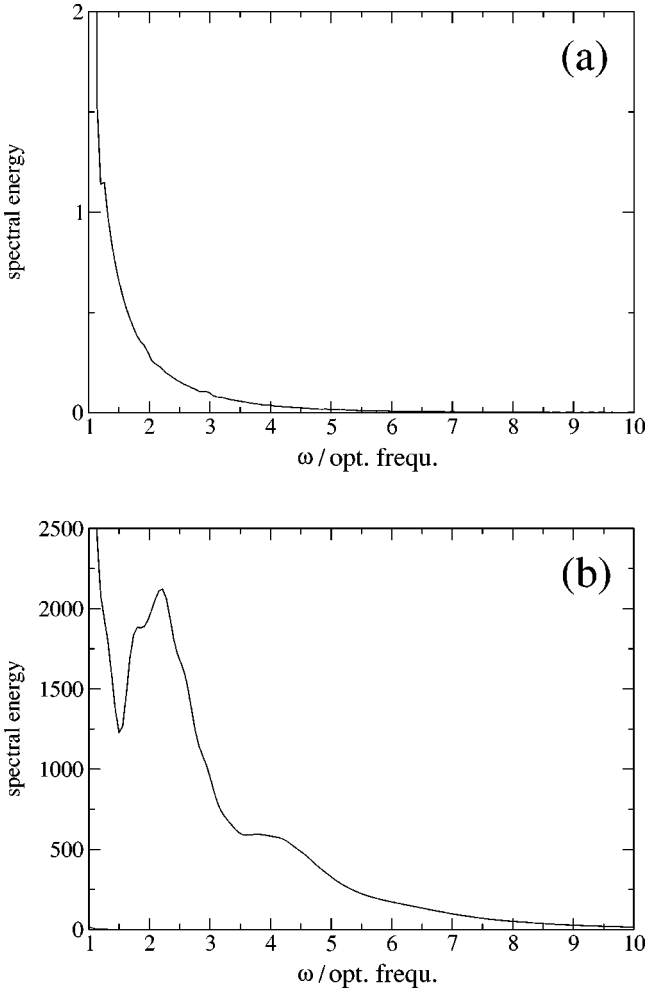

FIG. 6. Comparison of the spectral energy of the emitted light obtained from a first order perturbation theory proposed in [15] (a) and from the wave packet model presented in this work (b). The field parameters are $E_0=0.845$, $\omega=0.5$, $\sigma=6\pi/\omega$ and $t_0=9.66\pi/\omega$. The frequency is shown in units of the frequency of the external field.

and by approximating the initial ground state by a Gaussian. In this work the authors arrive at Eqs. (24) and (25) where the parameters are determined by the field-free motion of the wave packet $\mathbf{r}(t)=\int_0^t \mathbf{E}(t')dt'$ and $\rho(t)=\sqrt{\rho(\mathbf{0})^2+t^2/\rho(\mathbf{0})^2}$. By demanding a maximal overlap between the initial Gaussian and the exact ground-state wave function they obtained $\rho(\mathbf{0})=1.35/Z$, which slightly differs from Eq. (11) $\rho(\mathbf{0})=1.33/Z$. In Fig. 6 we compare the spectral energy of the emitted light obtained from Eqs. (24) and (25) with the calculations in [15]. The results are much different. In Fig. 6(a) the strength of higher harmonics decreases rapidly due to the monotone increase of the wave packet spreading. In contrast to this first order perturbation result, the spectral energy in Fig. 6(b) clearly shows a generation of higher order harmonics. Since the ionization rate is large for the used laser parameters, the efficiency of higher harmonic generation is low. Thus, the sharp plateau structure of the energy spectrum cannot be observed in the BSI regime. In Fig. 6(b) we can identify a weak plateau until a

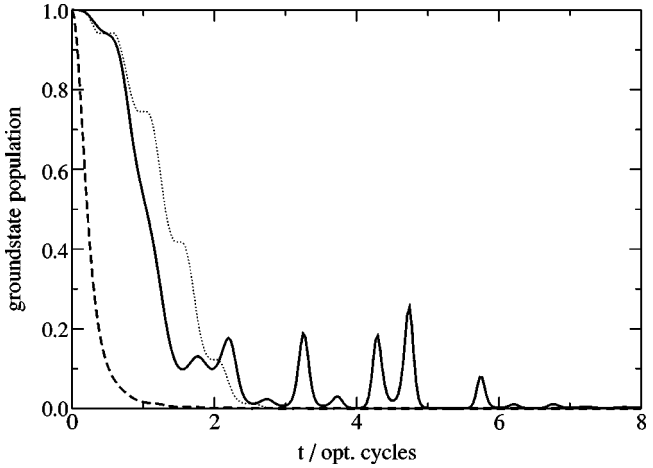

FIG. 7. Ground-state population as a function of time obtained from the presented wave packet model (solid line), from the first order perturbation approach of [20] (dashed line), and from the quantum formula obtained in [18] (dotted line). The field parameters are the same as in Fig. 6. The time is shown in units of the period length of the external field.

frequency of $\omega_c=4.5\omega$. This frequency corresponds to an energy of 2.25 a.u., which is equal to $2.63U_p+0.5$, where $U_p=E_{max}^2/4\omega^2$ is the maximum ponderomotive energy. Notice that this result differs by 17.8% from the $3.2U_p+E_B$ law for the higher harmonic cutoff in the tunneling ionization regime, which has been verified in various experiments and by theoretical studies [19]. As well known the generation of these higher harmonics is due to recombination of the residual ion and the electron that moves under the influence of the external field in the vincinity of the nucleus. This can be seen from the peaks occurring in the time evolution of the ground-state population (see Fig. 7). As can be also seen in Fig. 7, the ground-state population calculated from the Coulomb-free wave packet dynamics according to the first order perturbation approach in [15,20] disagrees with the formula in [18] and the recombination peaks completely disappear, which explains the absence of higher harmonics in Fig. 6. In [20] excellent agreement between the Coulomb-free wave packet dynamics and numerical solutions of the time-dependent Schrödinger equation has been found, for the case of a one-dimensional smoothed short range potential. But as we have shown, this approach fails to predict the ionization behavior of a three-dimensional Coulomb atom, which underlines again the importance of the properties of the used model potential.

A detailed study of these effects including interference effects and extending the model to the tunneling regime is subject to future work. However, the above investigations show that the wave packet model known from plasma physics is applicable in strong field atomic physics beyond the BSI regime. Having established the applicability of the semiclassical wave packet model to atom-light interaction we now study the electron dynamics from a more general point of view. Not all the following semiclassical results are essential for real quantum-mechanical situations, but nevertheless they give interesting insight into the complex dynamical properties of the atomic system.

III. DISSIPATIVE DYNAMICS

Up to this point the atom is considered as an isolated system only interacting with the laser field. Now we embed the model atom in a system consisting of many subsystems of the same type as our single atom to model a dense plasma. Each electron may carry out a free motion or is bound to its nucleus. Due to the interaction with this enviroment the electron is subject to dissipation. A full description of the dissipative processes requires the formulation of a quantum kinetic theory for atoms embedded into a plasma as given, e.g., by Klimontovich [21]. Such a complicated approach is beyond the scope of this paper. Here we prefer, therefore, a semiphenomenological approach, which is based on approximative solutions of the kinetic equations assuming weak deviations of the plasma from equilibrium. This so-called Spitzer approach is described, for example, in [21,22]. As a result the complicated interaction between the moving electron and the plasma is described by a linear friction term, which is introduced into the Hamiltonian dynamics [Eq. (10)],

$$\dot{p}_i = -\frac{\partial H}{\partial r_i} - \gamma p_i . \tag{26}$$

The friction constant γ is somehow related to the frequency of the collisions with the surrounding electrons. In the framework of the kinetic theory the average collision frequency may be estimated by the formula

$$\gamma = \frac{4\sqrt{2\pi} n e^4 L}{3 m_e (kT)^{3/2}}. \tag{27}$$

Here n is the density of charges in the plasma, m_e is the electron mass, T is the plasma temperature, and L is the so-called Coulomb logarithm [22]

$$L = \ln\left(\frac{k_{max}}{k_{min}}\right), \tag{28}$$

where k_{max} and k_{min} are the maximal and minimal values of the Coulomb collision parameter [21,22]. The non-Hamiltonian character of the system leads to the existence of attracting invariant sets in the phase space [23], which will be investigated now for atomic forces obtained from the variational principle.

A. Formation of attractors and bifurcation scenarios

In order to get significant qualitative effects we have chosen a rather large friction constant $\gamma = 0.05$ a.u. In this large damping regime the system is mainly moving on a stable final state (attractor), except for field strengths where the atomic potential does not play an essential role for the electron dynamics. But we found that there are very long chaotic transients before the system is cascading into the attractor. To check whether these transients are indeed chaotic, we have calculated the largest Lyapunov exponent, which measures the exponential divergence of initially nearby trajectories. The positive Lyapunov exponents obtained for the transients

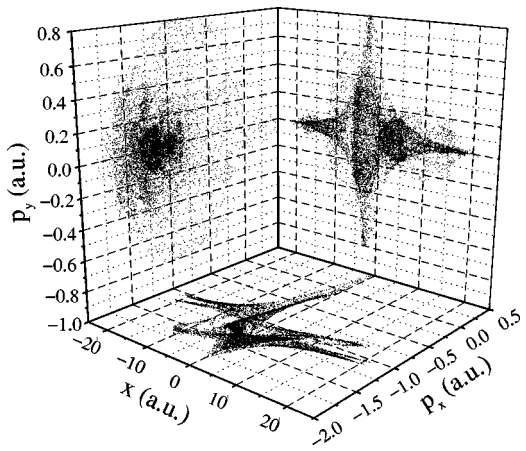

FIG. 8. Projection of a stroboscopic Poincaré section onto the three-dimensional phase space for $E_0 = 0.25$, $\omega = 0.23$, and $\gamma = 0.05$.

correspond to chaotic dynamics. The lifetime of these transients increases with a decreasing damping factor γ. Such chaotic transients were investigated by several authors [24–26] and were also found in the dynamics of trapped atoms [27]. During this transient process there is a high energy flow from the laser field to the electron, where the electron is thrown far out of the center. Due to the action of the atomic force and the dissipative effects it moves back to the nucleus. Such a chaotic transient is shown in Fig. 8 for certain field parameters. Note the large amplitude of the electron motion along the external field, which exceeds 20 a.u. for the used parameters. Since the oscillation perpendicular to the polarization direction of the laser field is also excited, the corresponding expectation value of the dipole moment has a nonvanishing value, in contrast to the Coulomb-free motion. Additionally, the chaotic character of the electron oscillation causes higher frequencies in the spectrum of the electron dipole radiation for all components of the dipole moment $\mathbf{d}(\mathbf{t})$.

Nonlinear dynamical systems often exhibit many rich and varied behavior of which stationary, periodic, quasiperiodic, and chaotic attractors are some of the typical long-term behaviors. A general approach in studying the complexity of such systems involves investigating their dynamics as some system parameters are varied. This method of analyzing qualitative changes in the systems' dynamics, known as bifurcations, yield a deeper insight into the global dynamics of the system. Bifurcations are sudden changes in the dynamics that occur when a system's parameter crosses a critical threshold. Such dynamical transitions result in one or more of the following changes.

(1) A change in the number and stability of different long-term behaviors, such as in a turning point or saddle node bifurcation, where a pair of a stable and an unstable stationary, periodic or quasiperiodic solutions, respectively, appears or disappears and as in a pitchfork bifurcation, where one stable solution loses stability and two new stable solutions with different symmetry properties appear.

(2) A stability change accompanied by a change in the type of behavior such as in (i) a torus bifurcation where a periodic solution loses stability and a stable quasiperiodic

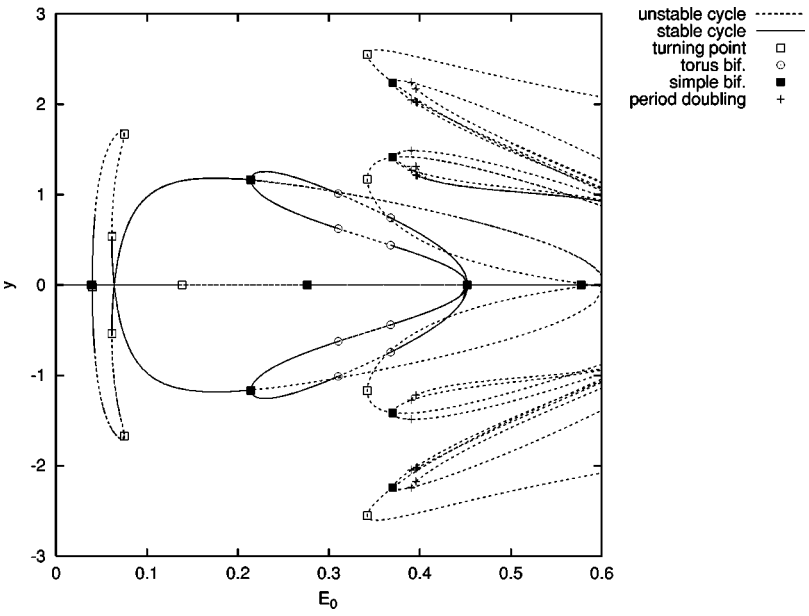

FIG. 9. Bifurcation diagram at $\omega=0.34$ a.u. and $\gamma=0.05$ a.u.

motion arises, (ii) a frequency locking, where the two frequencies of a quasiperiodic motion become rationally related leading to a periodic motion on the torus, and (iii) in a period doubling, where a periodic solution with period T becomes unstable and a periodic solution with double period $2T$ arises.

All the mentioned transitions can be found in the model for the dynamics of the electron studied in this paper. Moreover, we find also more complicated transitions, e.g., the appearance and disappearance of chaotic attractors.

Let us now study the dynamics of the system under variation of a system's parameter. Depending on E_0, ω, and γ the system exhibits a large variety of different long-term behavior, e.g., periodic, quasiperiodic, and chaotic motion. In some regions of the parameter space several attractors coexist. We cannot expect that all the fine details of the properties of the dynamical system have an important relevance for the real quantum-mechanical system. But the crucial differences in the behavior of the semiclassical atom at certain bifurcation points influence physical observables calculated from the trail wave function [Eq. (7)]. We will point out the essential features in the following at certain places. Let us discuss the behavior for a fixed external frequency ω and varying E_0. A bifurcation diagram characterizing the system's behavior with respect to the varying parameter E_0 is shown in Fig. 9. In the shown parameter interval the limit cycles can be divided into two classes, one-dimensional oscillations along the polarization direction of the applied electromagnetic field and two-dimensional limit cycles where the second oscillator perpendicular to the polarization direction is also excited. The one-dimensional oscillation becomes unstable at the turning point at $E_0=0.139$. This solution should become stable again at a turning point at $E_0=0.04$ in the case of only one driven oscillator. But we find that very near to this turning point, a pitchfork bifurcation occurs where the stable two-dimensional oscillation meets the unstable one-dimensional solution. The occurrence of the two-dimensional oscillation is due to internal resonance between both oscillators. The existence of transverse oscillations is the most important feature of the system. Thus analytical predictions about the occurrence of the coupled ocsillations would be important for applications to real physical problems. But an analytical study of both oscillators including the internal resonance as well as the resonance with the external field is very complicated and common methods do not describe the observed behavior. To simplify the problem we use the fact that the two-dimensional oscillation occurs at the second turning point and consider only the one-dimensional directly driven oscillator. At first we expand the atomic potential in the following form:

$$V(\boldsymbol{r})=A+\tfrac{1}{2}\omega_0^2 r^2-\tfrac{1}{4}\omega_0^2\alpha r^4+O(r^6). \tag{29}$$

By using this form the behavior of the oscillator near the main resonance can be studied by using a common perturbation theory. We obtain two turning points (Fig. 10) given by

$$\frac{E_0^2}{\kappa_{1/2}(\beta_0-\omega)^2}=\frac{\gamma^2}{4}+\left[\omega-\omega_0\left(1-\frac{3}{8}\alpha\kappa_{1/2}\right)\right]^2, \tag{30}$$

where

$$\kappa_{1/2}=\frac{8}{9\omega_0\alpha}\left(2(\omega_0-\omega)\pm\sqrt{(\omega_0-\omega)^2-\frac{3}{4}\gamma^2}\right). \tag{31}$$

This result will be discussed and compared with numerical calculations later. With a further increase in the external force the bifurcation behavior becomes relatively complicated. Figure 9 shows the corresponding bifurcation diagram using a stroboscopic Poincaré section projected onto the y axes. As mentioned above, for small field amplitudes less than 0.04 a.u. there is no coupling between oscillators transverse and in parallel with the polarization axes of the external field. The attractor is a symmetric circle in the x-y plane. If the external force increases, a symmetry breaking bifurcation occurs at a pitchfork bifurcation and two limit cycles

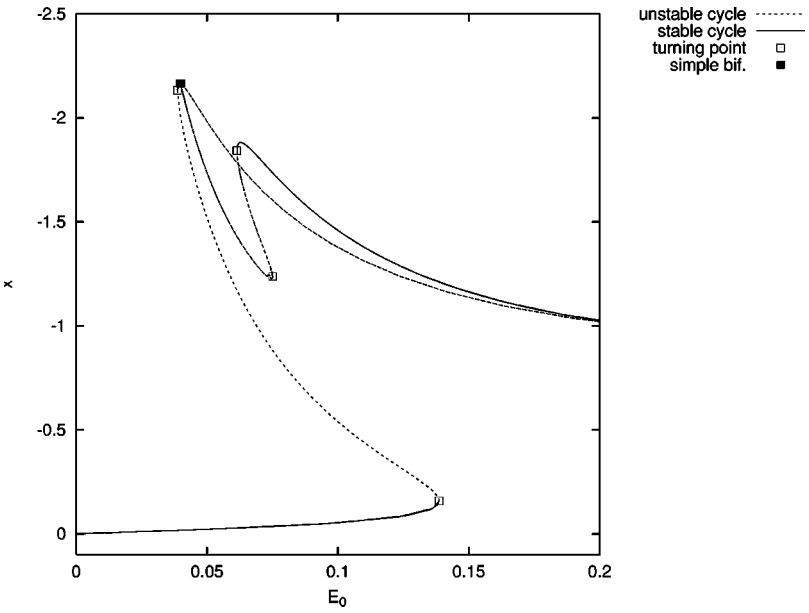

FIG. 10. Bifurcation diagram at $\omega = 0.34$ a.u. and $\gamma = 0.05$ a.u.

occur, which are symmetric to each other. For 0.04 a.u. $\leqslant E_0 \leqslant 0.139$ a.u. both solutions coexist in phase space. At $E_0 = 0.214$ a.u. the symmetry is broken again due to the generation of higher harmonics, so that from each attractor two new ones appear. A further increase in the external force leads to a torus bifurcation at $E_0 > 0.311$ a.u. Here the dynamics is characterized by oscillations with incommensurate frequencies and thus the trajctory lies on a torus. In certain parameter intervals a frequency locking on the torus can be resolved numerically (Fig. 11). For 0.34 a.u. $\leqslant E_0 \leqslant 0.353$ a.u. the motion of the electron becomes chaotic. Outside this interval the system settles on one of the four tori arising from the four asymmetric limit cycles. As can be seen in Fig. 11 it may happen that the system jumps to another torus due to the distortion in the chaotic regime. At $E_0 > 0.368$ a.u. a reverse torus bifurcation takes place and the four limit cycles become stable with increasing force. For higher field strength the motion is dominated by the external force. Thus, a single harmonic oscillation along the external field results for $E_0 > 0.44$ a.u. As mentioned above the spectrum of the dipole radiation calculated from the trail wave function [Eq. (7)] crucially depends on the different kinds of attractors. For the one-dimensional single harmonic oscillations ($E_0 < 0.04$ a.u. and $E_0 > 0.44$ a.u.) only one peak at the external frequency can be found in the spectrum of $d_x(t)$ and $\tilde{d}_y(\omega) = 0$. After the first pitchfork bifurcation (0.04 a.u. $< E_0 <$ 0.214 a.u.) single harmonic radiation along the y axes is obtained. For field strength of 0.214 a.u. $< E_0 <$ 0.311 a.u. peaks at higher frequencies $n\omega$ ($n \epsilon N$) are observed. In the quasiperiodic regime (0.311 a.u. $< E_0 <$ 0.368 a.u.) many peaks at higher and lower frequencies appear in the spectrum. For the case of frequency locking one finds peaks at lower frequencies ω/n whereas in the chaotic regime a broad frequency band is observed.

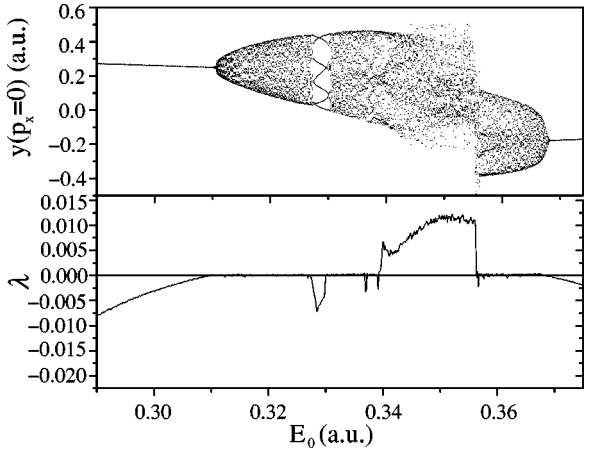

FIG. 11. Same as Fig. 7, but in a different representation. The stability is also shown in the form of Lyapunov exponents.

The discussed bifurcation scenario is a typical one for intermediate external frequencies between 0.25 a.u. and 0.4 a.u. However, these frequencies are not very realistic for actual experimental conditions. Typical lasers can reach frequencies of about 0.2 a.u. In this frequency regime the electron dynamics shows much differences compared to the case of higher frequencies. The field strength necessary to free the electron decreases with a decreasing frequency, which is in agreement with the stabilization effects in the Hamiltonian case discussed in the first part. Thus, finite attractors exist only for relatively low field strength where only the uncoupled single harmonic solution can be found. From a Taylor expansion of the atomic potential one can see that limit cycles with a period $T = n2\pi/\omega$ and arbitrary n should be possible. One can check the existence of such additional limit cycles by integrating the system with a large number of different initial conditions. Each of the attractors has its own basin of attraction. These basins are the sets of initial conditions, which all converge to this particular attractor. But the size of the basins of attraction of these limit cycles depend strongly on the parameters. Thus, in the higher frequency

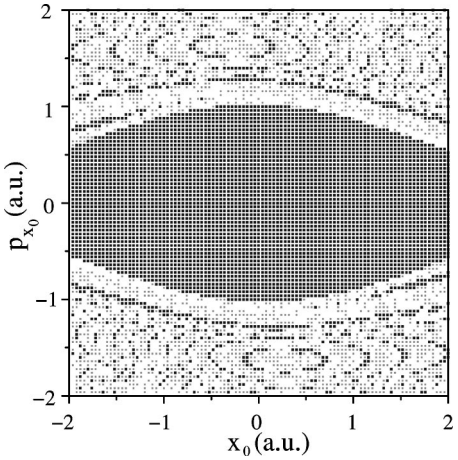

FIG. 12. Basin of attraction in the $x(t=0)-p_x(t=0)$ plane. $y(t=0)-p_y(t=0)$ are set to zero. Limit cycles with period 1 (black dots), 2 (gray dots), 3 and 4 (white area) are shown. The field parameters are $E_0=0.1$ a.u. and $\omega=0.4$ a.u..

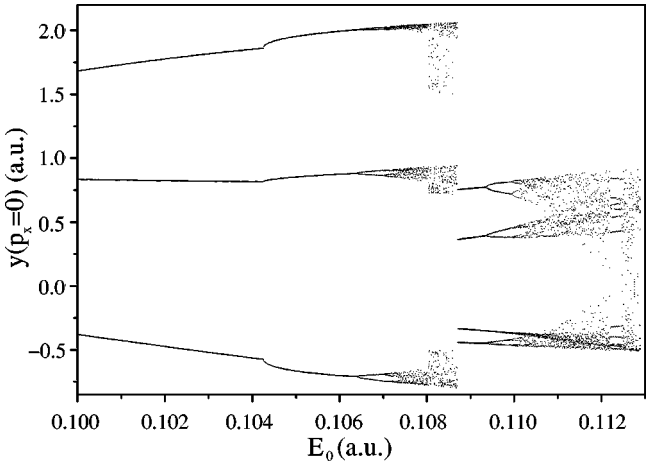

FIG. 13. Bifurcation diagram at $\omega=0.22$ a.u. and $\gamma=0.05$ a.u.

regime the limit cycles with higher periods cannot be observed numerically due to their small basins of attraction. Similar results have been found for mechanical oscillators [28]. For frequencies around 0.2 a.u. subharmonic resonances can be obtained. In Fig. 12 we show such a basin of attraction for $\omega=0.23$ and $E_0=0.1$. The boundaries of the basins of attraction have a fractal structure with a box counting dimension $d_F=1.733\pm0.003$, which has been computed using the uncertainty exponent [29]. Thus a small perturbation leads to a transition between the limit cycles. This has some consequences for the quasistatic tunneling model proposed in [19]. Here it is assumed that during the laser pulse at each time step a wave packet with positive energy is formed. In this work quantities, such as, the electron energy spectrum or the spectrum of the emitted light are calculated from the Coulomb-free wave packet dynamics and averaging the result over time by using the quasistatic tunneling ionization probability at each time step. But in the presented case due to the action of the Coulomb potential and the surroundings (dissipation), the time evolution of the wave packet strongly depends on the initial wave packet parameters and the initial phase of the laser field. From Fig. 12 one can see that in most of the cases the electron will oscillate with the external frequency. But nevertheless there are finite contributions to the wave packet motion with higher period lengths. If we follow the limit cycles with a higher period than $\omega/2\pi$ the transition into the chaotic dynamics occurs via period doubling. The chaotic attractor disappears again in a boundary crisis, e.g., the attractor collides with the boundary of its own basin of attraction. Figure 13 shows such a typical bifurcation diagram for a frequency of 0.22 a.u.

The complicated bifurcation behavior makes a detailed analysis of all bifurcation scenarios in the whole parameter space practically impossible. Thus we have to choose interesting pieces to characterize the dynamics of the system. In the following we only discuss the case of limit cycles with a period length $T=2\pi/\omega$. A rough bifurcation diagram for $\gamma=0.05$ is shown in Fig. 14. The solid lines correspond to bifurcations of the one-dimensional oscillations and dotted lines to those of the coupled motions. The different types of bifurcations are denoted by different letters. The analytical predictions for the two branches of turning points obtained from Eq. (30) are also shown (thin solid line). The agreement with the numerical calculations is very good. With Eq. (30) we can compare the shape of the two bifurcation lines for the three different potentials (Fig. 15). The behavior for the ''fixed width'' approximation and for the SAA potential is, in principle, the same whereas the branches for the ''soft-core'' potential are much more different. This is due to the differences in the linear coefficient obtained from an expansion of the potential [see Fig. 1(b)]. The such as structures like the Arnol'd tongues, which have to be situated at line *c*, cannot be resolved by our numerical techniques. However, the frequency locking shown in Fig. 8 indicates the existence of these tongues. Several routes into a chaotic regime are also shown in Fig. 14. For field strengths between $E_0=0.19$ and $E_0=0.39$ a transition occurs via a torus bifurcation in the case of coupled oscillations. At higher fields the two-dimensional oscillations undergo a period doubling cascade

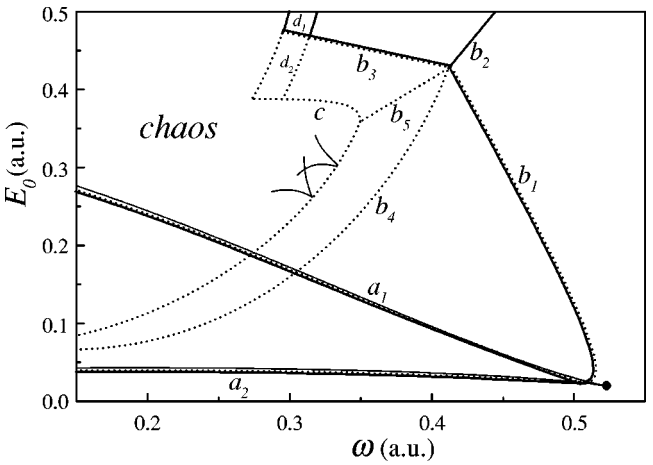

FIG. 14. Two-dimensional bifurcation diagram at $\gamma=0.05$ a.u. Branches of turning points (a), simple bifurcation points (b), torus bifurcation points (c), and period doubling points (d) are shown. Only the tongues at the torus bifurcation line are sketched.

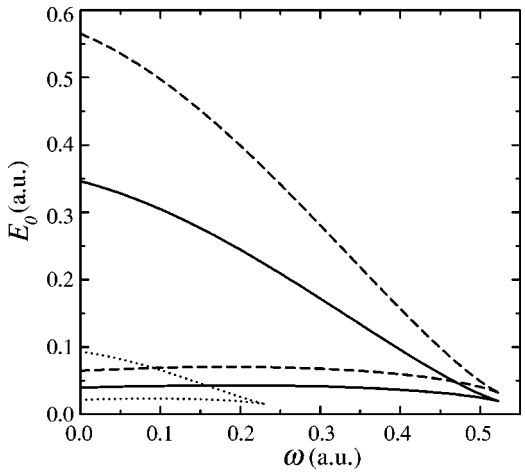

FIG. 15. Branches of two turning points at $\gamma=0.05$ a.u. for the ''fixed width'' approximation (solid lines), SAA potential (dashed lines), and ''soft-core'' potential (dotted lines).

at line d_2. The uncoupled limit cycles become chaotic via a period doubling cascade, denoted as line d_1 in the bifurcation diagram. At lower frequencies the torus bifurcation line meets the pitchfork bifurcation line outside the frame of Fig. 14 and a bifurcation of codimension 2 appears in the two-dimensional parameter space. Beyond this point the transition to chaos occurs via period doubling bifurcations. Another important point in Fig. 14 is the so-called cusp point at $E_0=0.02$ and $\omega=0.523$ where two branches of turning points meet. The cusp point can be calculated from Eq. (30). From the condition $\kappa_1=\kappa_2$ follows

$$\omega^{cusp}=\omega_0-\frac{\sqrt{3}}{2}\gamma,$$

$$E_0^{cusp}=\sqrt{\frac{2\sqrt{3}}{27}\frac{\gamma^3}{\omega_0\alpha}(\sqrt{3}\gamma-4\omega_0)^2}. \tag{32}$$

From this relation a critical damping constant follows

$$\gamma^c=\frac{2}{\sqrt{3}}\omega_0, \tag{33}$$

which corresponds to a critical plasma density n_e^c [see Eq. (27)]. For friction constants (or densities) larger than this critical value, the two turning point bifurcations vanish and the transverse oscillator is completely damped out.

The amplitudes of oscillations perpendicular to the polarization axes of the external field can exceed 2 a.u. This fact is of importance for the semiclassical description of higher harmonic generation and double ionization of multielectron atoms [19,30]. Here the electron dynamics after ionization is described by the Coulomb-free motion of a classical particle [30] or a wave packet [19]. At the time of encounter with its parent nucleus inelastic scattering is possible, which is connected with recombination leading to the emission of high frenquency light. In the case of multielectron atoms remaining electrons can also be ionized during the scattering process. But, as we have shown, the influences of the nonlinearities of the atomic potential will cause oscillations transverse to the field direction, which reduce the scattering probability by many orders of magnitudes. For damping constants larger than γ^c and frequencies larger than γ^{cusp} this effect plays no role. A comparison of the critical friction constants and frequencies for a characteristic friction is given in Table I. The ''soft-core'' potential leads again to much different results.

TABLE I. Critical damping constant γ^c for the three different potenials and ω^{cusp} for $\gamma=0.05$.

	γ^c	ω^{cusp}
SAA	0.564	0.523
Fixed width	0.564	0.523
Soft core	0.425	0.325

B. Influence of noise

Certainly the simple semiclassical atom model studied here fails to describe a real atom embedded in a surrounding, which is an open quantum system. However, at present, it seems to be hopeless to solve the full density operator equations for real atoms in strong fields and in a heat bath. Therefore, drastic approximations are necessary. Many effects, such as, the generation of higher harmonics [3] or strong field photoionization [31] can be described by a semiclassical approach, where an initial wave packet is propagated by the classical action $S(q,p)$ [32]. The fine structure of the classical dynamics gets lost in this semiclassical technique. We expect that those properties which survive under a stochastic perturbation may play a role in the semiclassical propagation of the electron state. In the following, we try to model the influence of the surrounding heat bath on the atom by inclusion of a stochastic force into the quasiclassical dynamical equations. We describe this force by a white noise term

$$\langle\xi_i(t)\rangle=0;\langle\xi_i(t)\xi_j(t')\rangle=2D\delta(t-t')\delta_{ij}, \tag{34}$$

which has to be added to Eq. (26). Then, the equations of motion are of Langevin type,

$$\dot{p}_i=-\frac{\partial H}{\partial r_i}-\gamma p_i+\xi_i(t). \tag{35}$$

The strength of the stochastic force may be connected with the damping constant and a formal temperature T of the heat bath with the help of the fluctuation-dissipation theorem

$$D=\gamma k_B T. \tag{36}$$

This stochastic force can also be seen as a simple model for the electric microfields in plasmas. In the case of dense plasma, which corresponds to high damping factors, these stochastic fields give the main contribution to ionization effects [33]. To study the influence of the noise we calculated again the bifurcation diagram shown in Fig. 9 by using Eqs. (9) and (11). The result is shown in Fig. 16. The fine struc-

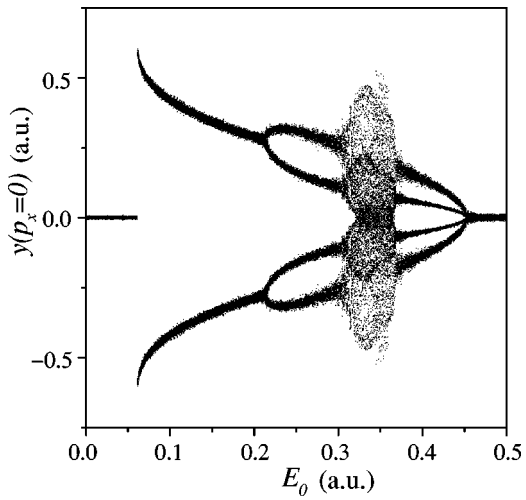

FIG. 16. Bifurcation diagram at $\omega=0.34$ a.u., $\gamma=0.05$ a.u., and $D=0.005$ a.u.

ture, such as the frequency locking on the torus, is completely destroyed. But we also see the conservation of symmetry breaking bifurcations due to resonances of the external field with both the transverse and the parallel oscillator. Thus, the combined action of the Coulomb potential and the surrounding fields (dissipation and fluctuation) leads to a dramatic reduction of the rescattering probability, which crucially influences the emission of light and the ionization process, as described in the last section.

IV. CONCLUSIONS

We have investigated the dynamics of a one-electron system in a nonlinear atomic potential under the action of an external periodical driving force. We considered a quasiclassical model of the electron dynamics based on the approach of wave packet dynamics in combination with a ''local Ritz principle.'' The results have been compared to the more familar ''soft-core'' potential. The advantage of the ''soft-core'' potential is the possibility to tune every ground-state energy wanted. But whereas the ''soft-core'' potential is introduced *ad hoc*, the present potential can be derived from a variational principle using an adiabatic approximation. A comparison of both potentials showed that differences in the linear as well as in the nonlinear terms lead to a very different electron dynamics. This result demonstrates how important the inclusion of finer details into models of atom dynamics is. The present model of electron dynamics, which is based on variational principles, shows a rich scenario of bifurcations in dependence on the strength and the frequency of the external field.

[1] C.K. Law, Q. Su, and J.H. Eberly, Phys. Rev. A **44**, 7844 (1991).
[2] M. Gavrila, in *Photon and Electron Collisions with Atoms and Molecules*, edited by P.G. Burke and C.J. Joachain (Plenum Press, New York, 1997).
[3] G. van de Sand and J.M. Rost, Phys. Rev. Lett. **83**, 524 (1999).
[4] D. Klakow, C. Toepffer, and P.G. Reinhard, Phys. Lett. A **192**, 55 (1994).
[5] J.P. Hansen and I.R. McDonald, Phys. Rev. A **23**, 2041 (1981).
[6] W. Ebeling and F. Schautz, Phys. Rev. E **56**, 3498 (1997).
[7] W. Ebeling, A. Förster, and V. Podlipchuk, Phys. Lett. A **218**, 297 (1996).
[8] W. Ebeling and B. Militzer, Phys. Lett. A, 298 (1996).
[9] W. Ebeling, T. Pohl, and J. Holyst, Laser Phys. **10**, 1069 (2000).
[10] H. Feldmeier, K. Bieler, and J. Schnack, Nucl. Phys. A **586**, 493 (1995).
[11] J. Schnack, Physica A **259**, 49 (1998).
[12] H. Feldmeier, Nucl. Phys. A **515**, 147 (1990).
[13] A.H. Nayfeh and D.T. Mook, *Nonlinear Oscillations* (Wiley, New York, 1995).
[14] P. Salieres *et al.*, Science **292**, 902 (2001).
[15] M.V. Fedorov and J. Peatross, Phys. Rev. A **52**, 504 (1995).
[16] A. Scrinzi, M. Geissler, and Thomas Brabec, Phys. Rev. Lett. **83**, 706 (1999).
[17] C.H. Keitel and P.L. Knight, Phys. Rev. A **51**, 1420 (1995).
[18] D. Bauer and P. Mulser, Phys. Rev. A **59**, 569 (1999).
[19] P.B. Corkum, Phys. Rev. Lett. **71**, 1994 (1993).
[20] R. Grobe and M.V. Fedorov, Phys. Rev. Lett. **68**, 2592 (1992).
[21] Yu.L. Klimontovich, *Kinetic Theory of Nonideal Gases and Plasmas* (Pergamon Press, Oxford, London, 1982).
[22] W. Ebeling *et al.*, *Transport Properties of Dense Plasmas* (Birkhäuser, Basel, 1984).
[23] M.A. Lieberman and K.Y. Tsang, Phys. Rev. Lett. **55**, 908 (1985).
[24] J.A. Yorke and E.D. Yorke, J. Stat. Phys. **21**, 263 (1979).
[25] P. Holmes and D. Whitley, Physica D **7**, 111 (1983).
[26] H.W. Yin, J.H. Dai, and H.J. Zhang, Phys. Rev. Lett. **254**, 165 (1999).
[27] J.L. Shen, H.W. Yin, J.H. Dai, and H.J. Zhang, Phys. Rev. A **55**, 2159 (1997).
[28] U. Feudel, C. Grebogi, B.R. Hunt, and J.A. Yorke, Phys. Rev. E **54**, 71 (1996).
[29] S.W. McDonald, C. Grebogi, E. Ott, and J.A. Yorke, Physica D **17**, 125 (1985).
[30] M.Yu. Romanovsky, J. Ortner, V.V. Korobkin, and W. Ebeling, Laser Phys. **9**, 1 (1999).
[31] J. Ortner and V.M. Rylyuk, Phys. Rev. A **61**, 033403 (2000).
[32] M.F. Herman and E. Kluk, Chem. Phys. **91**, 27 (1984).
[33] J. Ortner and M.Yu. Romanovsky, Phys. Lett. A **285**, 165 (2001).